Available online at www.sciencedirect.com
SCIENCE DIRECT®
Journal of Sound and Vibration 291 (2006) 1186–1201
JOURNAL OF SOUND AND VIBRATION
www.elsevier.com/locate/jsvi

Supersonic flutter suppression of piezolaminated cylindrical panels based on multifield layerwise theory

I.K. Oh[a,*], I. Lee[b]

[a]*School of Mechanical Systems Engineering, Chonnam National University, 300 Yongbong-dong, Puk-gu, Gwang-Ju 500-757, Republic of Korea*
[b]*Division of Aerospace Engineering, Department of Mechanical Engineering, Korea Advanced Institute of Science and Technology, 373-1 Kusong-Dong, Yusong-Gu, Taejoin 305-701, Republic of Korea*

Received 2 May 2005; received in revised form 11 May 2005; accepted 15 July 2005
Available online 9 September 2005

Abstract

For the aerothermoelastic analysis of cylindrical piezolaminated shells, geometrically nonlinear finite elements based on the multifield layerwise theory have been developed. Present multifield layerwise theory describes zigzag displacement, thermal and electric fields providing a more realistic multiphysical description of fully and partially piezolaminated panels. By applying a Hans Krumhaar's supersonic piston theory, supersonic flutter analyses are performed for the cylindrical piezolaminted shells subject to thermal and piezoelectric loads. The possibility to increase flutter boundary and reduce thermoelastic deformations of piezolaminated panels is examined using piezoelectric actuation. Results show that active piezoelectric actuation can effectively increase the critical aerodynamic pressure by retarding the coalescence of flutter modes and compensating thermal stresses.

1. Introduction

The recent emergence of smart structure technology capable of the enhancement of the static and dynamic stabilities has led to application of active or semi-active control to many systems. Numerous studies on the smart structures using piezoelectric materials are focused on vibration

*Corresponding author. Tel./fax: +82 62 530 1685.
E-mail address: ikoh@chonnam.ac.kr (I.K. Oh).

0022-460X/$ - see front matter © 2005 Elsevier Ltd. All rights reserved.
doi:10.1016/j.jsv.2005.07.033

Nomenclature

a, b	panel length, width
h	thickness of panels
h_{BASE}	thickness of base composite panel
σ_{ij}	Cauchy stress tensor
f_i	body forces
τ_i	surface traction
ρ	density of structures
ρ_{a}	density of airflow
u_i	displacements
D_i	electric displacement vector
q	electric body charge
C_{ijkl}	elastic material properties
$\in_{ik}$	dielectric constant
e_{kij}	piezoelectric coefficient
α_{ij}	thermal expansion coefficient
p_i	pyroelectric constants
E_k	electric field vector
ΔT_k	temperature rise in kth layer
φ	electric potential
U^J, V^J	in-plane displacement at the Jth interface
W	transverse displacement
$\Phi^J(z)$	linear Lagrangian interpolation
R	radius of cylindrical shells
g	distance from x-axis to arbitrary point
ϕ	shallowness angle
θ	fiber angle
Q_{ij}	elastic modulus
$\bar{Q}_{ij}$	reduced elastic modulus
$\bar{e}_{ij}$	reduced piezoelastic constant
$\bar{\psi}_k$	shape function
M	Mach number
$\mathbf{u}$	displacement vector
$\mathbf{M}$	mass matrix
$\mathbf{K0}$	linear stiffness matrix
$\mathbf{KN1}$	first-order nonlinear stiffness matrix
$\mathbf{KN2}$	second-order nonlinear stiffness matrix
$\mathbf{K}^{\Delta T}$	thermal geometric matrix
$\mathbf{K}^{\mathrm{P}}$	piezoelectric geometric stiffness
$\mathbf{F}^{\Delta T}$	thermal loading
$\mathbf{F}^{\mathrm{P}}$	piezoelectric actuation forces
Ψ	eigen-mode vector
D	rigidity of panel
β	aerodynamic pressure parameter
μ	aerodynamic damping parameter
γ	curvature term in Hans Kurmhaar's piston theory

and static shape controls. Especially, the applications of piezoelectric material and shape memory alloy to the bucking control are found in several studies. Meressi and Paden [1] designed an LQR controller for the effective buckling control of a beam. Thompson and Loughlan [2] performed an experimental study on the active bucking control of a column with surface bonded piezoelectric materials. Faria and Almeida [3] investigated the enhancement of pre-buckling behavior of composite beams with geometric imperfections using piezoelectric actuators. Oh et al. [4,5] reported thermopiezoelastic postbuckling and snap-through behaviors of piezolaminated plates using layerwise nonlinear finite elements. They firstly found a secondary instability such as snap-through due to excessive piezoelectric actuation to suppress thermally buckled deflections.

Also, the studies on the aeroelastic enhancement using piezoelectric materials have been reviewed. Ehlers and Weisshaar [6] altered the aeroelastic behaviors in terms of the divergence and the lift effectiveness applying piezoelectric anisotropic induced strain. Song et al. [7] examined a wing model of composite thin-walled beam with embedded active layers considering the transverse shear and secondary warping. Lin and Crawley [8] developed analytical models based on the Rayleigh–Ritz approach to investigate aeroelastic control using piezoelectric induced strain and LQR control. Scott and Weisshaar [9] proposed a linear panel flutter control using piezoelectric actuators and sensors. Zhou et al. [10] investigated the effective suppression of the

nonlinear panel flutter. Frampton et al. [11] studied an active control of panel flutter including fully linearized potential flow aerodynamic theory appropriate for the full transonic and low supersonic range. Dongi et al. [12] used output feedback control from a pair of collocated or self-sensing piezoactuators for the active compensation of aerodynamic stiffness to suppress a panel flutter. Recently, Suleman [13] investigated supersonic flutter suppression and noise control of composite shells using piezoelectric materials.

Most studies concerning the smart structures for aeroelastic enhancement have been limited to the flat plate model, whereas the active flutter suppression is realistically applicable to the curved skin structures subject to thermal stresses. In this study, the supersonic panel flutter of piezolaminated cylindrical panels subject to thermal and piezoelectric loads is investigated by applying geometrical nonlinear finite element method based on the multifield layerwise theory.

2. Finite element formulations

The converse and direct linear piezoelectric constitutive equations with steady-state temperature fields are expressed in the following form:

$$\sigma_{ij} = C_{ijkl}\varepsilon_{kl} - e_{kij}E_k - \alpha_{ij}\Delta T, \tag{1}$$

$$D_i = e_{ikl}\varepsilon_{kl} + \in_{ik} E_k + p_i \Delta T, \tag{2}$$

where ε_{ij}, E_k and ΔT denote Green–Lagrange strain tensor, electric field vector and temperature increase. C_{ijkl}, e_{kij} and $\in_{ik}$ are elastic, piezoelectric and dielectric constants. And α_{ij} and p_i are thermal–mechanical and thermal–piezoelectric coupling constants. Here, the electric field vector E_k is related to electric field potential φ:

$$E_i = -\varphi_{,i}. \tag{3}$$

The variational form of the equation of motion for admissible virtual displacement δu_i and potential $\delta\varphi$ is given as follows:

$$\delta T - \delta H + \delta W_{\text{ex}} = 0. \tag{4}$$

Here, T, H and W_{ex} are the kinetic energy, electromechanical energy and the work of external mechanical and electric body and surface forces and charges, defined by the following expressions:

$$T = \frac{1}{2}\int_V \rho \dot{u}_i \dot{u}_i \,\mathrm{d}V, \tag{4a}$$

$$H = \frac{1}{2}\int_V (\sigma_{ij}\varepsilon_{ij} - D_i E_i)\,\mathrm{d}V, \tag{4b}$$

$$W_{\text{ex}} = \int_V f_i u_i \,\mathrm{d}V + \int_S \tau_i u_i \,\mathrm{d}S - \int_V q\varphi \,\mathrm{d}V - \int_S Q_E \varphi \,\mathrm{d}S. \tag{4c}$$

In Eq. (4), the major difference from the variational form of the pure structures is an electromechanical coupling. The full electromechanical coupling in Eq. (4) could be handled with both mechanical displacements and electric potentials.

For a body of referential volume V and of referential surface S with prescribed forces on a part of S and prescribed geometric boundary conditions on the remaining surface that has undergone an infinitesimal virtual displacement, δu_i, we have

$$-\int_V \rho \ddot{u}_i \delta u_i \, dV - \int_V (\sigma_{ij}\delta\varepsilon_{ij} - D_i \delta E_i) \, dV + \int_V f_i \delta u_i \, dV + \int_S \tau_i \delta u_i \, dS - \int_V q\delta\varphi \, dV - \int_S Q_E \delta\varphi \, dS = 0, \tag{5}$$

where σ_{ij} are elements of the second Piola–Kirchhoff stress tensor. Also, τ_i and Q_E mean prescribed stresses and electric surface charge.

Based on the multifield layerwise theory, the elastic displacements (u, v and w), electric potentials, and temperature fields on the $x-\phi-z$ material coordinate system shown in Fig. 1, can be expressed by introducing the following piecewise continuous approximations as follows:

$$u_1 = u(x, \phi, z, t) = \sum_{J=1}^{N_i} U^J(x, \phi, t)\Phi^J(z), \tag{6}$$

$$u_2 = v(x, \phi, z, t) = \sum_{J=1}^{N_i} V^J(x, \phi, t)\Phi^J(z), \tag{7}$$

$$u_3 = w(x, \phi, z, t) = W(x, \phi, t) \tag{8}$$

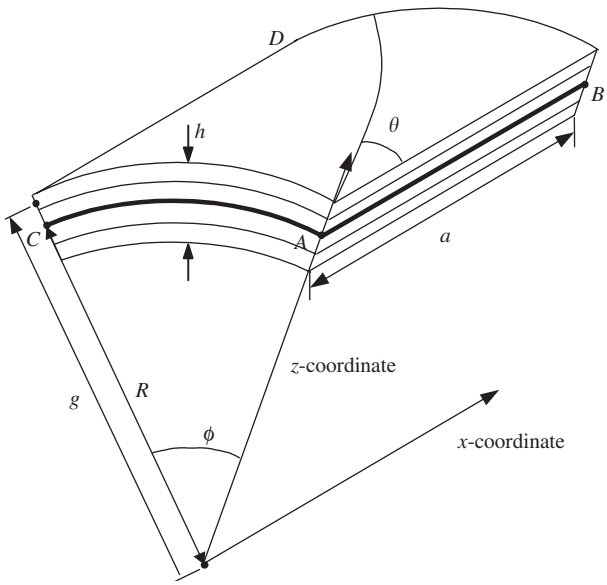

Fig. 1. Geometry of cylindrical composite shell.

and

$$\Delta T(x,\phi,z,t)=\sum_{J=1}^{N_i}\Delta T^J(x,\phi,t)\Phi^J(z), \tag{9}$$

$$\varphi(x,\phi,z,t)=\sum_{J=1}^{N_i}\varphi^J(x,\phi,t)\Phi^J(z), \tag{10}$$

where U^J, V^J, ΔT^J and φ^J are axial and hoop displacements, temperature increase and electric potential at the Jth interface; N_i is the number of degrees of freedom for the in-plane displacement along the thickness direction for the element i; $\Phi^J(z)$ is the Lagrange interpolation function [14].

The von-Karman nonlinear relationship between strains and displacements is applied to consider a large deflection due to aerodynamic and thermopiezoelectric loads as follows:

$$\varepsilon_{xx}=\frac{\partial u}{\partial x}+\frac{1}{2}\left(\frac{\partial w}{\partial x}\right)^2=\sum_{J=1}^{N_i}\frac{\partial U^J}{\partial x}\Phi^J+\frac{1}{2}\left(\frac{\partial W}{\partial x}\right)^2, \tag{11}$$

$$\varepsilon_{\phi\phi}=\frac{\partial v}{g\partial\phi}+\frac{w}{g}+\frac{1}{2}\left(\frac{\partial w}{g\partial\phi}\right)^2=\sum_{J=1}^{N_i}\frac{\partial V^J}{g\partial\phi}\Phi^J+\frac{W}{g}+\frac{1}{2}\left(\frac{\partial W}{g\partial\phi}\right)^2, \tag{12}$$

$$\gamma_{x\phi}=\frac{\partial u}{g\partial\phi}+\frac{\partial v}{\partial x}+\frac{\partial w}{\partial x}\frac{\partial w}{g\partial\phi}=\sum_{J=1}^{N_i}\left(\frac{\partial U^J}{g\partial\phi}+\frac{\partial V^J}{\partial x}\right)\Phi^J+\frac{\partial W}{\partial x}\frac{\partial W}{g\partial\phi}, \tag{13}$$

$$\gamma_{\phi z}=\frac{\partial w}{g\partial\phi}+\frac{\partial v}{\partial z}-\frac{v}{g}=\frac{\partial W}{g\partial\phi}+\sum_{J=1}^{N_i}V^J\frac{\mathrm{d}\Phi^J}{\mathrm{d}z}-\sum_{J=1}^{N_i}\left(\frac{V^J}{g}\right)\Phi^J, \tag{14}$$

$$\gamma_{xz}=\frac{\partial w}{\partial x}+\frac{\partial u}{\partial z}=\frac{\partial W}{\partial x}+\sum_{J=1}^{N_i}U^J\frac{\mathrm{d}\Phi^J}{\mathrm{d}z}. \tag{15}$$

Based on the Hans Krumhaar's modified supersonic piston theory [15] considering the curvature effect of cylindrical structures, the aerodynamic stiffness and damping matrices can be derived using the virtual work done by the aerodynamic pressure differential ΔP in the following form:

$$\begin{aligned}\Delta P &= -\frac{\rho_a U_\infty^2}{\sqrt{M^2-1}}\left\{\frac{\partial w}{\partial x}+\frac{1}{Ma_\infty}\left(\frac{M^2-2}{M^2-1}\right)\frac{\partial w}{\partial t}-\frac{1}{2R\sqrt{M^2-1}}w\right\}\\ &= -\beta\frac{\partial w}{\partial x}-\mu\frac{\partial w}{\partial t}+\gamma w,\end{aligned} \tag{16}$$

where M is the Mach number, and U_∞ is the freestream speed. And β, μ and γ are the aerodynamic pressure parameter, damping parameter and radius coefficient, respectively; w is the transverse deflection of skin panel. Here, one can obtain the aerodynamic force vector with

respect to finite element nodal displacements as follows:

$$\mathbf{F}^{\Delta P} = -\beta \mathbf{A}_\beta \mathbf{u} - \mu \mathbf{A}_\mu \dot{\mathbf{u}} + \gamma \mathbf{A}_\gamma \mathbf{u}. \tag{17}$$

Assuming linear variation of electric potential through the thickness direction, the induced potential can be neglected and electro-mechanical coupling will be partial. Especially, for the modeling of only actuation problems since the variations of electric fields components are zero and electric charge are not often considered, a variational thermopiezoelastic equation with a linear potential assumption can be easily obtained by using conventional Hamilton's principle. Through the assembly procedure, the global aerothermopiezoelastic finite element equation of the coupled dynamics can be obtained as follows:

$$\mathbf{M}\ddot{\mathbf{u}} + \mu \mathbf{A}_\mu \dot{\mathbf{u}} + \begin{pmatrix} \mathbf{K0} + \beta \mathbf{A}_\beta - \gamma \mathbf{A}_\gamma - \mathbf{K}^{\Delta T} \\ -\mathbf{K}^P + \frac{1}{2}\mathbf{KN1} + \frac{1}{3}\mathbf{KN2} \end{pmatrix} \mathbf{u} = \mathbf{F}^{\Delta T} + \mathbf{F}^P. \tag{18}$$

In order to analyze the aerothermopiezoelastic deflections and linear flutter boundaries, the solution of Eq. (18) is assumed to be the sum of time-dependent and time-independent solution such as $\mathbf{u} = \mathbf{u}_s + \mathbf{u}_t$, where $\mathbf{u}_s$ is the static large deflection and $\mathbf{u}_t$ is the time-dependent solution with small amplitude. Substituting this assumed solution into Eq. (18) and using the transformation such as $\mathbf{KN1}(\mathbf{u}_t)\mathbf{u}_s = \mathbf{KN1}(\mathbf{u}_s)\mathbf{u}_t$, we can obtain static and dynamic coupled two equations as follows:

$$\mathbf{q}(\mathbf{u}_s) = \begin{pmatrix} \mathbf{K0} + \beta \mathbf{A}_\beta - \gamma \mathbf{A}_\gamma - \mathbf{K}^{\Delta T} \\ -\mathbf{K}^P + \frac{1}{2}\mathbf{KN1}(\mathbf{u}_s) + \frac{1}{3}\mathbf{KN2}(\mathbf{u}_s) \end{pmatrix} \mathbf{u}_s - \mathbf{F}^{\Delta T} - \mathbf{F}^P = \mathbf{0}, \tag{19}$$

$$\mathbf{M}\ddot{\mathbf{u}}_t + \mu \mathbf{A}_\mu \dot{\mathbf{u}}_t + \begin{pmatrix} \mathbf{K0} + \beta \mathbf{A}_\beta - \gamma \mathbf{A}_\gamma - \mathbf{K}^{\Delta T} \\ -\mathbf{K}^P + \frac{1}{2}\mathbf{KN1}(\mathbf{u}_s) + \frac{1}{3}\mathbf{KN2}(\mathbf{u}_s) \end{pmatrix} \mathbf{u}_t = \mathbf{F}^{\Delta T} + \mathbf{F}^P, \tag{20}$$

where $\mathbf{q}(\mathbf{u}_s)$ is the out-of-balance force vector. The Newton–Raphson iteration method is used to solve the aerothermopiezoelastic static deflections from Eq. (19). For the $(i+1)$th iteration, an incremental equation can be written as

$$\begin{pmatrix} \mathbf{K0} + \beta \mathbf{A}_\beta - \gamma \mathbf{A}_\gamma - \mathbf{K}^{\Delta T} - \mathbf{K}^P \\ +\mathbf{KN1}(\mathbf{u}_s^i) + \mathbf{KN2}(\mathbf{u}_s^i) \end{pmatrix} \Delta \mathbf{u}_s^{i+1} = \Delta \mathbf{F}^i, \tag{21}$$

where

$$\Delta \mathbf{F}^i = \mathbf{F}^{\Delta T} + \mathbf{F}^P - \begin{pmatrix} \mathbf{K0} + \beta \mathbf{A}_\beta - \gamma \mathbf{A}_\gamma - \mathbf{K}^{\Delta T} - \mathbf{K}^P \\ +\frac{1}{2}\mathbf{KN1}(\mathbf{u}_s^i) + \frac{1}{3}\mathbf{KN2}(\mathbf{u}_s^i) \end{pmatrix} \mathbf{u}_s^i. \tag{22}$$

By solving Eq. (21), the updated displacement vector is determined as follows:

$$\mathbf{u}_s^{i+1} = \mathbf{u}_s^i + \Delta \mathbf{u}_s^{i+1}, \tag{23}$$

where $\mathbf{u}_s^{i+1}$ and $\Delta \mathbf{u}_s^{i+1}$ are the static and incremental displacements in the $(i+1)$th iteration.

The full system equations with skew symmetric aerodynamic matrix need very large DOF and computational cost. In order to reduce computational time and cost, the modal reduction is adopted to find a linear flutter speed in this study. The modal vectors are found at a static

equilibrium point under the given temperature distribution using the following eigen-value equation:

$$\begin{bmatrix} \mathbf{K0} - \mathbf{K}^{\Delta T} - \mathbf{K}^{P} - \omega^2 \mathbf{M} \\ +\mathbf{KN1}(\mathbf{u}_s) + \mathbf{KN2}(\mathbf{u}_s) \end{bmatrix} \Psi = \mathbf{0}. \tag{24}$$

The reduced flutter equation using modal approach can be obtained by

$$\mathbf{M}^* \ddot{U} + \mathbf{K}(\beta, \mathbf{u}_s)^* U = \mathbf{0}, \tag{25}$$

where

$$\mathbf{M}^* = \mathbf{\Psi}^T \mathbf{M} \mathbf{\Psi}, \tag{26}$$

$$\mathbf{K}(\beta, \mathbf{u}_s)^* = \mathbf{\Psi}^T \begin{pmatrix} \mathbf{K0} + \beta \mathbf{A}_\beta - \gamma \mathbf{A}_\gamma - \mathbf{K}^{\Delta T} - \mathbf{K}^{P} \\ +\mathbf{KN1}(\mathbf{u}_s) + \mathbf{KN2}(\mathbf{u}_s) \end{pmatrix} \mathbf{\Psi}. \tag{27}$$

The reduced stiffness matrix in Eq. (27) is reconstructed with increasing dynamic pressure (β) and converged displacement ($\mathbf{u}_s$). The linear flutter boundary can be determined by solving the complex eigen-value problem from Eq. (25) with increasing aerodynamic pressure. In many cases, the flat panel flutter occurs by the coalescence between (1,1) and (1,2) modes at critical aerodynamic pressure. Therefore, most analyst has used modal approach with 6–10 mode shapes in the aeroelastic analyses of flat panel. However, we used 30 mode shapes for more accurate results in the aeroelastic analyses of cylindrical composite panels from the results of convergence test because the flutter of cylindrical panels can occur at higher circumferential modes.

For a simple presentation of analysis results, the following non-dimensional parameters are introduced as

$$\beta^* = \beta \frac{a^3}{D}, \quad \omega^* = \omega_i \sqrt{a^4 \frac{\rho c}{D}}, \tag{28}$$

where β^* and ω^* are the non-dimensional dynamic pressure and frequency, respectively; a and h are axial length and typical thickness of skin panel, respectively; D is rigidity of panel as defined by $D = E_2 h^3$ for anisotropic material.

3. Verification of present FE codes

The first problem illustrates the response of cantilever [P/45/-45/0]s cylindrical shells with continuous PZT-4 layer attached on each side of the composite shells. The material properties are given in Table 1. The thickness of a lamina is 0.24 mm, whereas the thickness of each piezoelectric layer is 0.24 mm. The circumferential length $b = R\phi = 0.314$ m and the aspect ratio $b/a = 5$ remain constant. The mid-surface radius R is varied to study of the effects of a curvature on the active response of the shell. The shell configurations are shown in Fig. 2 with a cylindrical coordinate system.

The active response is induced by applying electric potentials of $+100$ V on the free surface of each piezoceramic, resulting in out-of-phase actuations. The effect of curvature, expressed by the

Table 1
Material properties of Graphite-Epoxy, Titanium, and PZTs

Properties	Graphite/Epoxy	PZT-5A	Titanium	PZT-4
E_1 (GPa)	150	63	114	81.3
E_2 (GPa)	9.0	63	114	81.3
E_3 (GPa)	9.0	63	114	64.5
G_{12} (GPa)	7.1	24.2	43.846	30.6
G_{13} (GPa)	7.1	24.2	43.846	25.6
G_{23} (GPa)	2.5	24.2	43.846	25.6
v_{12}	0.3	0.3	0.3	0.329
v_{13}	0.3	0.3	0.3	0.43
α_1 (10^{-6}/°C)	1.1	0.9	—	—
α_2 (10^{-6}/°C)	25.2	0.9	—	—
d_{ij}				$e_{31} = -5.20$
(10^{-12} m/V)		$d_{31} = 254$		$e_{31} = -5.20$
Or	—	$d_{32} = 254$	—	$e_{33} = 15.08$
e_{ij}				$e_{24} = 12.72$
(C/m^2)				$e_{15} = 12.72$
ρ (kg/m^3)	1600	7600	2768	7600
Room temp. (°C)	20	20	20	20

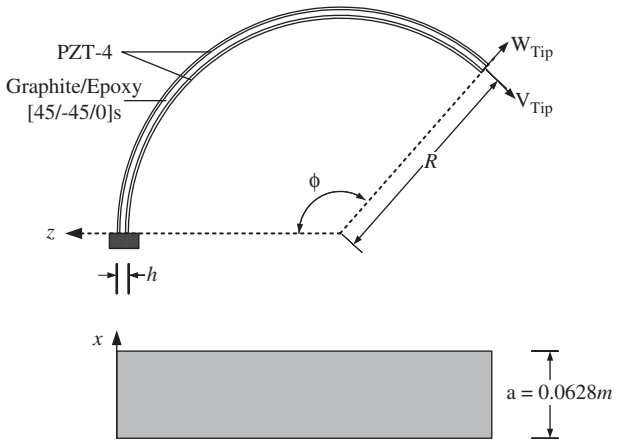

Fig. 2. Circular cantilever shell with piezoelectric active layers.

ratio h/R, on the active tip deflection of the shell is shown in Fig. 3. Present results are compared with the results of Saravanos [16] by mixing layerwise electric potential field with first-order shear displacement theory, the so-called MPST. Present results based on the multifield layerwise theory has good agreements with the results of Saravanos on the range between $h/R = 0.0$ and 0.006. However, as the curvature ratio increases above $h/R = 0.006$, the difference between present results and MPST is observed. The present finite element model gives more accurate and flexible results by considering the zigzag in-plane DOFs than those by single layer theories.

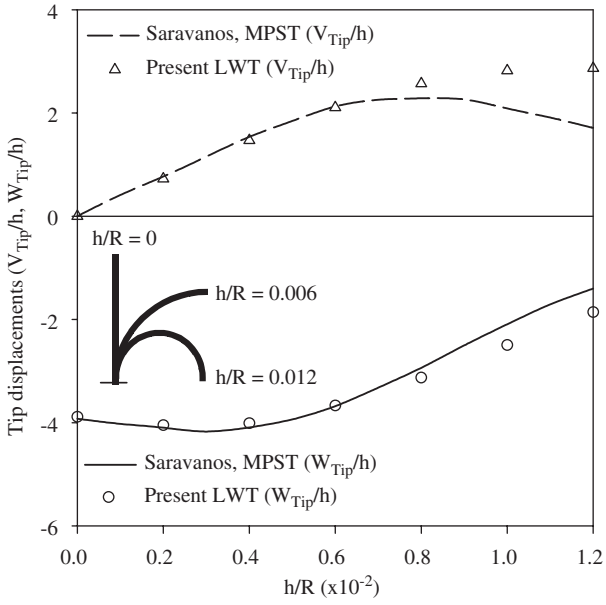

Fig. 3. Effect of curvature on the tip displacements of a piezolaminated shell.

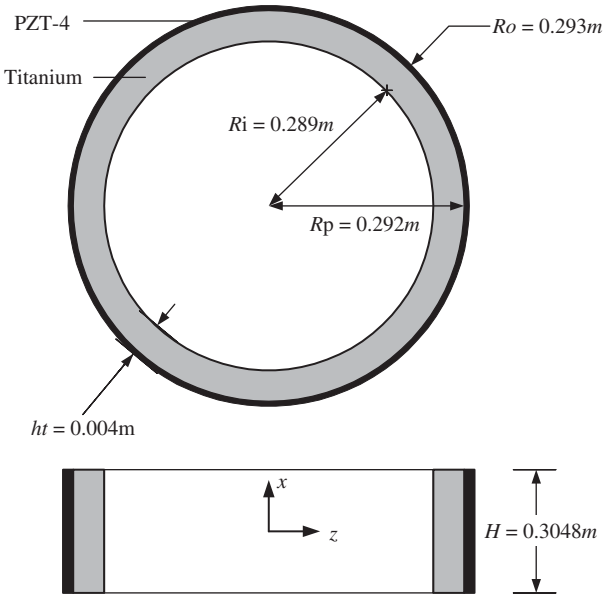

Fig. 4. Domain and geometry of circular cylindrical piezolaminated ring.

Next, a circular cylindrical piezo-laminated ring by Heyliger et al. [17] is examined. The geometry of the cylinder is described in cylindrical coordinates (x, ϕ, z), as shown in Fig. 4. The dimensions of the ring are defined by the height $H = 0.3048$ m, the inner radius $Ri = 0.289$ m, and

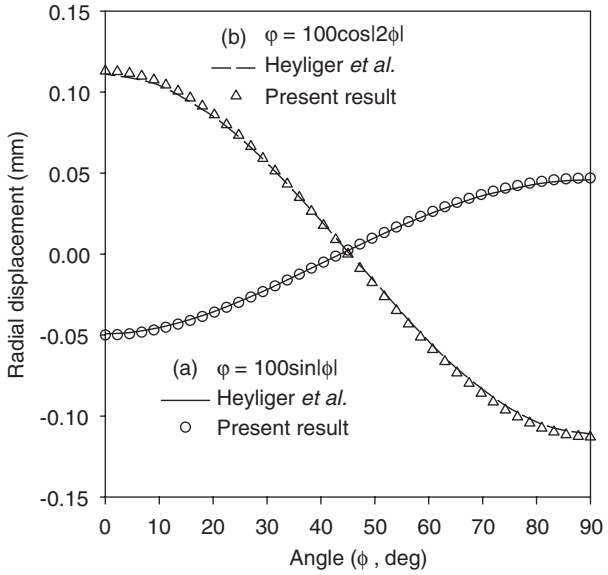

Fig. 5. Radial displacement distributions for applied surface potentials in circular cylindrical piezolaminated ring.

the total thickness $h_t = 0.004\,\text{m}$. The laminate has two layers: titanium and PZT-4. The thickness ratio of the titanium to the PZT-4 is fixed at 3. In the finite element analysis, one-quarter of the shell is typically modeled using the symmetry of geometry and load. A mesh discretization of 20×4 with nine-node elements is used for the symmetric model. For the verification of active static behavior, two surface potentials are applied in the quarter model as follows:

$$\text{Case (a)} \quad \varphi(\phi) = 100 \sin|\phi|, \quad 0 \leqslant \phi \leqslant \frac{\pi}{2}, \tag{29}$$

$$\text{Case (b)} \quad \varphi(\phi) = 100 \cos|2\phi|, \quad 0 \leqslant \phi \leqslant \frac{\pi}{2}. \tag{30}$$

In each case, the potential at the inner surface of the active layer is fixed at zero. Present results are in excellent agreement with the results of Heyliger et al. [17] as shown in Fig. 5.

4. Results and discussion

During last decade, a few research papers have been reported in the research field for the aeroelastic control of supersonic flutter responses using smart materials. In this study, semi-active flutter suppressions of cylindrical composite panels are investigated using piezoelectric materials.

Consider a cylindrical $[(90_2/0_2)\text{s}/\text{P}]$ panel with piezoceramic patches as shown in Fig. 6. Here, P means active piezoelectric layer. The basic geometry consists of axial length $a = 1\,\text{m}$, inner radius $R = 0.5\,\text{m}$, and shallowness angle $\phi = 60^\circ$. The clamped boundary conditions are imposed on the edge of $\widehat{AB}$ and $\widehat{CD}$. And the simply supported boundary conditions are also imposed on the edge

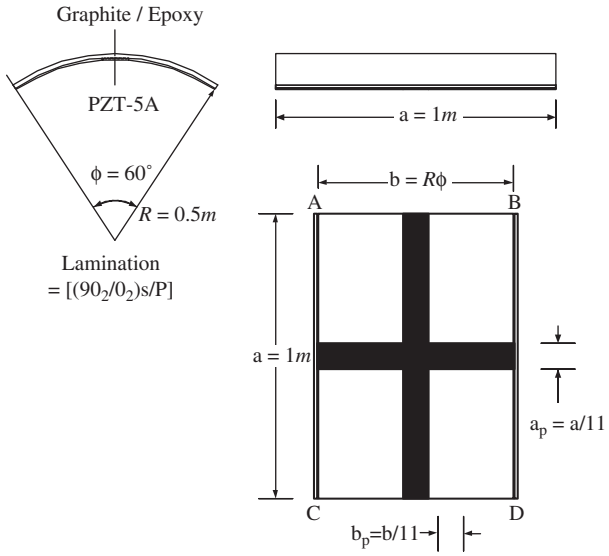

Fig. 6. Geometry of piezolaminated cylindrical panel.

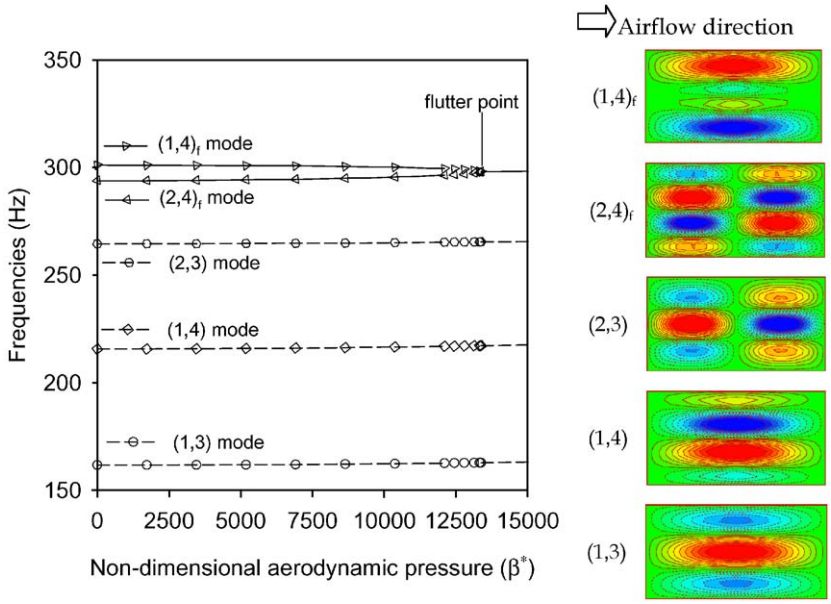

Fig. 7. Mode coalescence and mode shapes of piezolaminated cylindrical panels without active actuation.

of $\overline{AC}$ and $\overline{BD}$. Material properties used in this study are Graphite/Epoxy and PZT-5A given in Table 1. The thickness of a composite lamina is 0.125 mm and the thickness of PZT is 0.2 mm, resulting in the total thickness of 1.2 mm. At a flutter point, two eigenmodes of the cylindrical panels merge and lead to dynamic instability because of aerodynamic pressure forces on the panel. The piezoceramic patches are cruciform so as to efficiently delay the coalescence of flutter modes

as shown in Fig. 7. Also, in order to avoid the change of external airflow from patch-type actuators, active piezoceramic layers are only attached to inner surface of cylindrical composite panels.

In the first place, let us investigate the linear flutter characteristics of piezolaminated cylindrical panels without piezoelectric actuation. The mode coalescence between $(2,4)_f$ and $(1,4)_f$ mode shapes leads to a self-excited oscillation, namely panel flutter, as shown in Fig. 7. Here, a non-dimensional aerodynamic pressure is defined by Eq. (28). The thickness of base composite laminates except a piezoceramic layer is used in the calculation of bending stiffness $D = E_2 h_{\mathrm{BASE}}^3$. The thickness used in the non-dimensional aerodynamic pressure is $h_{\mathrm{BASE}} = 1.0\,\mathrm{mm}$.

It is well known that aeroelastic stabilities can be improved by piezoelectric actuation. The frequencies of piezolaminated cylindrical panels are changed by active piezoelectric actuation as shown in Fig. 8. The lower five modes are compared: the variation of natural frequencies by piezoelectric actuation of $\varphi = 100$ and $-100\,\mathrm{V}$ is very slight, and the actuations by $\varphi = 100$ and $200\,\mathrm{V}$ slightly increase the frequency interval of flutter modes of $(2,4)_f$ and $(1,4)_f$. However, the active actuation by $\varphi = 200\,\mathrm{V}$ can improve a critical aerodynamic pressure as shown in Fig. 9.

Though active control voltages of cruciform piezoelectric patches slightly increase the frequency interval of flutter modes, the critical aerodynamic pressure dramatically increases because of the retardation of coalescence between $(2,4)_f$ and $(1,4)_f$ modes. Consequently, a simple semi-active methodology to enhance the flutter boundary is to increase the frequency interval of flutter modes, or to suppress the mode coalescence.

The thermoelastic responses of composite cylindrical panels with patch-type piezoelectric materials are different from those of pure composite panels. In this section, the thermoelastic behavior, vibration characteristics and flutter mechanism of a piezolaminated cylindrical panel are

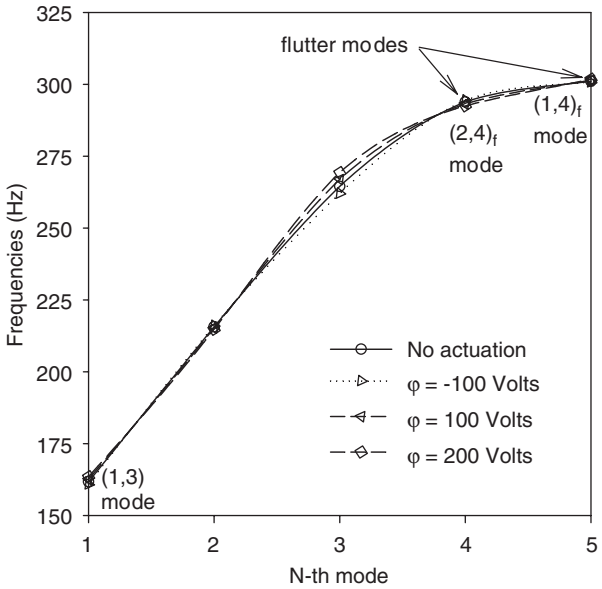

Fig. 8. Frequency variations of cylindrical panels for lower five modes according to piezoelectric actuation.

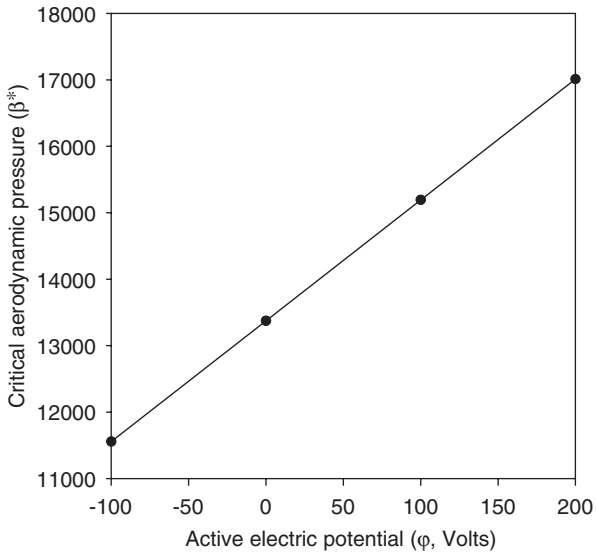

Fig. 9. Linear flutter boundary of piezolaminated cylindrical panels by active actuation.

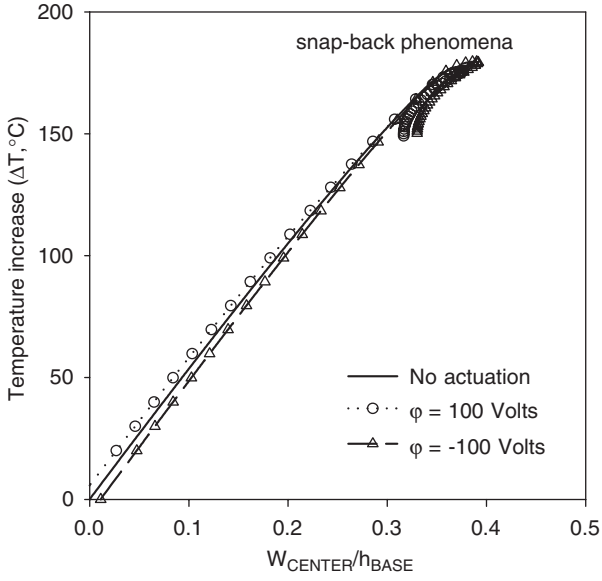

Fig. 10. Thermoelastic deflection of piezolaminated cylindrical panels with snap-back phenomenon.

investigated. Here, the temperature distribution is assumed to be uniform along the thickness direction. First, the results of thermoelastic responses are shown in Fig. 10. The snap-back phenomena occur in the nonlinear thermoelastic responses. The piezoelectric actuation can reduce

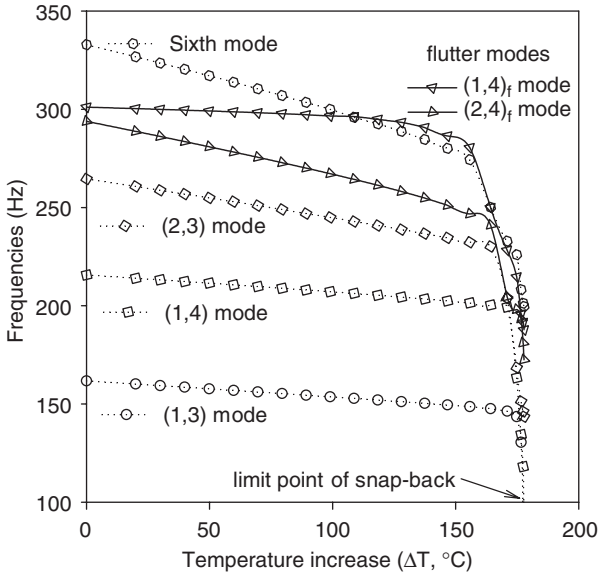

Fig. 11. Frequency history of piezolaminated cylindrical panel according to temperature increase.

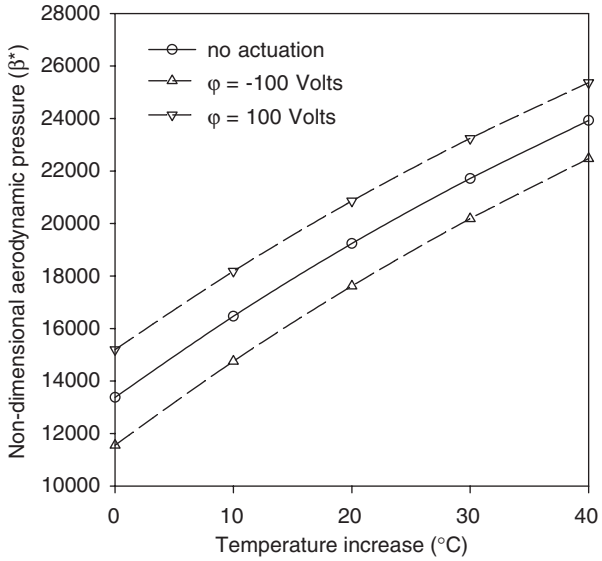

Fig. 12. Flutter boundaries of piezolaminated cylindrical panels subject to thermal stresses according to piezoelectric actuation.

and increase static deformations, whereas it is very difficult to suppress a snap-back phenomenon [5,14] of shell type structures because of low piezoelectric forces and nonlinear dynamics.

Most external skins of supersonic/hypersonic rockets, launch vehicles and aircrafts experience severe environmental conditions such as high temperatures and aeroacoustics. Many studies have

addressed the aerothermoelastic instabilities of plates. The critical aerodynamic pressures of flat panels can be reduced by thermal stresses. Also, in the cylindrical composite panel, the dramatic drop of flutter boundaries of a composite cylindrical panel subject to thermal stresses have been observed in our previous study. However, unlike flat panel, some structural models of piezolaminated cylindrical panels subject to thermal stresses shows that on the contrary the critical aerodynamic pressure increases with increasing temperatures. It is due to the increase of frequency interval of flutter modes with increasing temperatures. As shown in Fig. 11, the frequency interval of $(2,4)_f$ and $(1,4)_f$ modes of the piezolaminated cylindrical panels increases according to temperature increases. Those phenomena result in the increase of critical aerodynamic pressure of piezolaminated cylindrical panels subject to thermal stresses as shown in Fig. 12. Also, results show that the piezoelectric actuation by $\varphi = 100\,\mathrm{V}$ can also increase critical aerodynamic pressure, where the active response by $\varphi = -100\,\mathrm{V}$ can also decrease flutter boundaries of cylindrical composite panels subject to thermal stresses.

In this study, a simple model is investigated to increase critical aerodynamic pressure of cylindrical composite panels subject to thermal stresses. Unlike the suppression of static deformations, present cruciform piezoelectric patches can simply increase the flutter boundary by inducing the retardation of coalescence of flutter modes.

5. Conclusion

The geometrically nonlinear finite elements based on the multifield layerwise theory have been developed in order to improve thermoelastic deformations and supersonic flutter characteristics of the cylindrical composite panels in supersonic flow region. Present multifield layerwise theory describes zigzag displacement, thermal and electric fields providing a more realistic multiphysical description of fully and partially piezolaminated panels when compared to the equivalent single layer theories.

It is well known that the thermal stresses weaken the flutter stability of flat panel resulting in a flutter dip at a certain temperature distribution. However, present results show that on the contrary the critical aerodynamic pressure of some structural models of piezolaminated cylindrical panels increases as the surface temperature increases. It is due to the increase of the frequency interval of flutter modes with increasing temperatures.

Also, the possibility to increase flutter boundary and reduce thermoelastic deformations of piezolaminated panels is examined using piezoelectric actuation. Results show that active piezoelectric actuation can effectively increase the critical aerodynamic pressure of piezolaminated cylindrical panels by retarding the coalescence of flutter modes and compensating thermal stresses.

References

[1] S. Meressi, B. Paden, Buckling control of a flexible beam using piezoelectric actuators, *Journal of Guidance, Control, and Dynamics* 16 (1993) 977–980.

[2] S.P. Thomson, J. Loughlan, The active buckling control of some composite column strips using piezoceramic actuators, *Composite Structures* 32 (1995) 59–67.
[3] A.R. Faria, S.F.M. Almeida, Enhancement of pre-buckling behavior of composite beams with geometric imperfections using piezoelectric actuators, *Composites Part B: Engineering* 30 (1999) 43–50.
[4] I.K. Oh, J.H. Han, I. Lee, Postbuckling and vibration characteristics of piezolaminated composite plate subject to thermopiezoelectric loads, *Journal of Sound and Vibration* 233 (2000) 19–40.
[5] I.K. Oh, J.H. Han, I. Lee, Thermopiezoelastic snapping of piezolaminated plates using layerwise nonlinear finite elements, *AIAA Journal* 39 (2001) 1188–1198.
[6] S.M. Ehlers, A. Weisshaar, Static aeroelastic behavior of an adaptive laminated piezoelectric composite wing, *AIAA Journal* 28 (1990) 1611–1623.
[7] O. Song, L. Librescu, C.A. Rogers, Application of adaptive technology to static aeroelastic control of wing structures, *AIAA Journal* 30 (1992) 2882–2889.
[8] C.Y. Lin, E.F. Crawley, Toward optimal aeroelastic control using elastic and induced strain anisotropy, *Proceedings of the 38th AIAA/ASME/ASCE/AHS/ASC Structures, Structural Dynamics, and Material Conference* 3 (1994) 1781–1792.
[9] R.C. Scott, T.A. Weisshaar, Controlling panel flutter using adaptive materials, *Journal of Aircraft* 31 (1994) 213–222.
[10] R.C. Zhou, Z. Lai, D.Y. Xue, J.K. Huang, C. Mei, Suppression of nonlinear panel flutter at elevated temperature with piezoelectric actuators, *AIAA Journal* 33 (1995) 1098–1105.
[11] K.D. Frampton, R.L. Clark, E.H. Dowell, Active control of panel flutter with piezoelectric transducers, *Journal of Aircraft* 33 (1996) 768–774.
[12] F. Dongi, D. Dinkler, B. Kroplin, Active panel flutter suppression using self-sensing piezoactuators, *AIAA Journal* 34 (1996) 1224–1230.
[13] A. Suleman, Adaptive composites modelling and applications in panel flutter and noise suppression, *Computers & Structures* 76 (2000) 365–378.
[14] I.K. Oh, I. Lee, Thermal snapping and vibration characteristics of cylindrical composite panels using layerwise theory, *Composite Structures* 51 (2001) 49–61.
[15] H. Krumhaar, The accuracy of linear piston theory when applied to cylindrical shells, *AIAA Journal* 1 (1963) 1448–1449.
[16] D.A. Saravanos, Mixed laminated theory and finite element for smart piezoelectric composite shell structures, *AIAA Journal* 35 (1997) 1327–1333.
[17] P. Heyliger, K.C. Pei, D. Saravanos, Layerwise mechanics and finite element model for laminated piezoelectric shells, *AIAA Journal* 34 (1996) 2353–2360.